Assessment of Existing CHF Correlations for the Operating Conditions and Design Region of the i-SMR

Seojun Park, Kyung Mo Kim*
Department of Energy Engineering, Korea Institute of Energy Technology (KENTECH),
Kentech-gil 21, Naju-si, Jeollanam-do 58330, Republic of Korea
*seojun@kentech.ac.kr, kmokim@kentech.ac.kr**

**Keywords : CHF, Small Modular Reactor, Rod bundle, Reactor Safety, Conservatism*

1. Introduction

When the local heat flux along the fuel rods in a reactor core exceeds the critical heat flux (CHF), heat transfer between the fuel rod and the coolant decreases sharply, leading to a rapid fuel-rod temperature increase and potential cladding failure [1]. Therefore, core thermal design is determined by the departure from nucleate boiling ratio (DNBR = q''_{CHF}/q''_{loc}).

The i-SMR, an innovative small modular reactor currently under design in Korea, differs from conventional large pressurized water reactors (PWRs) in three respects [2]: a short heated length of about 2.4 m, a low coolant mass flux of about 1,500 kg/m²·s, and a bottom-peaked axial power distribution resulting from soluble-boron-free operation.

CHF prediction under this combination of design characteristics has received little attention. Existing rod-bundle CHF correlations were developed from the conditions and design characteristics of large PWRs, and whether they retain their prediction performance under the i-SMR conditions remains to be confirmed.

In this study, the prediction performance of the B&W-2, W-3, and WRB-1 correlations is therefore assessed against the EPRI rod-bundle CHF database, which encompasses the i-SMR design and operating characteristics. The assessment identifies the parameter that limits the prediction performance under the i-SMR conditions, and the identification is then verified by refitting the corresponding term of the correlations.

2. Rod-bundle CHF Correlations

The B&W-2 and W-3 correlations combine a correlation developed under uniform heating conditions with a correction factor for non-uniform axial power distributions, whereas the functional form of the WRB-1 correlation has not been publicly disclosed and only its published variable dependence is described. The applicability ranges of the three correlations are summarized in Table 1, together with the licensed DNBR limit of each correlation, i.e., the minimum DNBR to be maintained in design so that DNB is avoided with a 95% probability at a 95% confidence level.

Table 1. Applicability ranges of the B&W-2 [3], W-3 [1], and WRB-1 [4] correlations (SI)

Parameter	B&W-2	W-3	WRB-1
Pressure (MPa)	12.07 - 16.89	6.90 - 15.86	9.93 - 17.17
Mass flux (kg/m²·s)	1,044 - 5,425	1,356 - 6,781	1,221 - 5,018
Local quality	-0.03 - +0.22	-0.25 - +0.15	-0.20 - +0.30
Equivalent diameter (mm)	5.08 - 13.31	5.08 - 17.78	9.40 - 15.24
Heated length (mm)	1,829 (fixed)	254 - 3,658	≤ 4,267
95/95 DNBR limit	1.30	1.30	1.17

2.1 B&W-2 Correlation

The B&W-2 correlation was developed by Gellerstedt et al. [3] from CHF data obtained in rod bundles cooled by pressurized water. It predicts CHF from the pressure P, the local mass flux G, the local quality x, the equivalent diameter D_e, and the latent heat of vaporization h_{fg}, and contains no inlet-condition term; the pressure enters through the exponents of the mass-flux terms. The B&W-2 correlation is expressed as follows (British units):

$$q''_{BW2},uni = (a - b \cdot D_e) \cdot \frac{[A_1 \cdot (A_2 \cdot G)^{p_1} - A_9 \cdot G \cdot x \cdot h_{fg}]}{[A_5 \cdot (A_6 \cdot G)^{p_2}]} \quad (1)$$

$$p_1 = A_3 + A_4 \cdot (P - 2000) \quad (2)$$

$$p_2 = A_7 + A_8 \cdot (P - 2000) \quad (3)$$

where $a = 1.15509, b = 0.40703\ \text{in}^{-1}$, $A_1 = 0.37020 \times 10^8, A_2 = 0.59137 \times 10^{-6}$, $A_3 = 0.83040$, $A_4 = 0.68479 \times 10^{-3}$, $A_5 = 12.710$, $A_6 = 0.30545 \times 10^{-5}$, $A_7 = 0.71186, A_8 = 0.20729 \times 10^{-3}$, and $A_9 = 0.15208$.

For a non-uniform axial power distribution, the uniform-heating CHF is divided by the correction factor F_D. F_D takes the same integral form as the Tong F-factor described in Section 2.2, but its decay constant C_{BW} was determined separately from the B&W-2 database and an additional multiplicative constant K_D= 1.02508 is applied. The integration extends from the channel inlet (z = 0) to the evaluation point L_{DNB}, and F_D reduces exactly to K_D under uniform heating:

$$F_D = \frac{K_D \cdot C_{BW} \cdot \int_0^{L_{DNB}} q''(z) \exp[-C_{BW}(L_{DNB} - z)] dz}{q''(L_{DNB})[1 - \exp(-C_{BW} L_{DNB})]} \quad (4)$$

$$C_{BW} = \frac{0.24867(1-x)^{7.82293}}{(G/10^6)^{0.45758}} \quad [\text{in}^{-1}] \quad (5)$$

2.2 W-3 Correlation

The W-3 correlation predicts CHF from the pressure P, mass flux G, local quality x, inlet subcooling $h_{sat} - h_{in}$, and the equivalent diameter D_e, based on experimental data obtained in single channels [1]. Its range of applicability is given in Table 1. The W-3 correlation is expressed as follows (British units):

$$q''_{W-3,Uni} = 10^6 \times k_1(P,x) \times k_2(x,G) \times k_3(x) \times k_4(D_e) \times k_5(\Delta h), \quad (6)$$
$$k_1 = (2.022 - 0.0004302P) + (0.1722 - 0.0000984P)e^{(18.177-0.004129P)x},$$
$$k_2 = (0.1484 - 1.596x + 0.1729x|x|)(G/10^6) + 1.037,$$
$$k_3 = 1.157 - 0.869x,$$
$$k_4 = 0.2664 + 0.8357e^{-3.151D_e},$$
$$k_5 = 0.8258 + 0.000794(h_f - h_{in}).$$

Since the axial power distribution of an actual core is non-uniform, Tong (1967) [1] derived the F-factor to extend $q''_{W-3,Uni}$ to non-uniform axial distributions. The derivation is based on an energy balance of the near-wall bubble layer: DNB is governed not only by the local heat flux but also by the upstream heating history accumulated in the bubble layer, whose contribution decays exponentially with distance from the DNB location. The F-factor is expressed as follows (British units):

$$q''_{W-3,Non} = \frac{q''_{W-3,Uni}}{F} \quad (7)$$

$$F = \frac{C\int_0^{L_{DNB}} q''(z)e^{-C(L_{DNB}-z)}dz}{(q''(L_{DNB})[1-e^{-C\cdot L_{DNB}}])} \quad (8)$$

$$C = \frac{0.15(1-x_{DNB})^{4.31}}{(G/10^6)^{0.478}}\ [in^{-1}] \quad (9)$$

where L_{DNB} is the distance from the onset of local boiling to the DNB evaluation point, z is the axial coordinate measured from the onset of local boiling, and x_{DNB} is the local equilibrium quality at the evaluation point.

2.3 WRB-1 Correlation

The WRB-1 correlation was developed by Motley et al. [4] exclusively from CHF data obtained in rod bundles with mixing vane grids. Its coefficients are proprietary and have not been published, whereas the functional form is known to be linear in the local quality:

$$q''_{WRB1} = A - Bx \quad (10)$$
$$A = A(P, G, L_h, g_{sp}, d_g)$$
$$B = B(P, G, L_h)$$

where L_h is the heated length, g_{sp} is the mixing vane grid spacing, and d_g is the distance from the evaluation point to the nearest upstream grid; the two grid-related terms represent the turbulence induced by the mixing vane grids, which decays with distance downstream. In contrast to the two correlations above, the WRB-1 correlation therefore contains the heated length and the grid spacing as explicit variables.

3. Methods

The assessment employs the EPRI rod-bundle CHF database compiled by Fighetti and Reddy [5], which provides, for each test, the geometry of the rod-bundle test section, the operating conditions (pressure, mass flux, and inlet temperature), and the measured CHF. The tests cover uniform and non-uniform axial power distributions and wide ranges of mass flux and heated length that include both the i-SMR and the PWR design regions. In total, 9,003 cases were analyzed with the subchannel analysis code MATRA [6] to obtain the axial and subchannel-wise distributions of the local conditions required by the correlations, and the 8,525 cases evaluated in common by all three correlations under both evaluation bases described below form the common sample of this study.

The prediction quality is measured by the predicted-to-measured CHF ratio *P/M*, where *P/M* > 1 corresponds to a non-conservative prediction. Two evaluation bases are used. In the direct substitution method (DSM), the local conditions at the experimental power are substituted into the correlation, and *P/M* is taken at the minimum-DNBR location over all rods and axial positions. In the heat balance method (HBM), the bundle power is scaled until the minimum DNBR reaches unity, and *P/M* is the resulting power ratio. The assessment of the correlations is performed on the HBM basis, which measures how well each correlation predicts the thermal margin of a given test; the refit is performed on the DSM basis, which isolates the prediction accuracy of the correlation itself at fixed local conditions and is therefore suited to re-fitting its coefficients. The *P/M* distributions are summarized by the median, the logarithmic standard deviation σ_{ln} and the non-conservative fraction.

Table 2. Design regions for the assessment (common pressure range of 12.0–16.5 MPa)

Region	*G* (kg/m²·s)	*L* (mm)
i-SMR region	1,250 - 1,600	≤ 2,438
PWR region	3,200 - 3,900	≥ 3,650

The analysis proceeds in four steps. First, the overall performance of the three correlations is examined on the common sample. The remaining steps are confined to the two design regions defined in Table 2 and to a common pressure range: the operating pressures of the two target designs are nearly identical (≈15.5 MPa), so the pressure acts as a controlled variable, and the lower bound of the range follows the applicability limit of B&W-2 in Table 1. Second, the effect of the axial power distribution is checked within each design region, by comparing uniform-heating and bottom-peaked (or mid-peaked) cases under matched conditions, to determine whether the mixture of axial power distributions distorts the region comparison that follows. Third, the correlations are assessed over each region in its entirety, irrespective of the applicability range of each correlation, because the i-SMR design actually resides in this region; the fraction of cases inside each applicability range is reported separately. The distribution of non-conservative

predictions is then examined over the parameter space to locate the region where each correlation weakens. Fourth, the correlation term associated with the identified weak axis is refitted, and the residual structure of the refitted correlation is examined. W-3 is selected as the refit target for two reasons. First, its functional form and coefficients are fully published, and its multiplicative structure allows an individual term to be modified while the remaining terms are kept intact, whereas the proprietary WRB-1 cannot be modified. Second, W-3 rests on the local conditions hypothesis: the uniform correlation, developed from single-channel data, predicts CHF from the local conditions at the point of interest, and bundle-specific effects enter only through separable correction factors; the correlation is therefore not tied to a particular bundle geometry, which leaves room for extension to new design conditions such as the i-SMR. B&W-2, the other published correlation, is refitted in the same manner as a control.

4. Results and Discussion

4.1 Overall Performance

Fig. 1 and Table 3 present the overall performance of the three correlations, evaluated on the common sample of 8,525 cases on the HBM basis; the dashed lines in Fig. 1 denote the medians, and the last column of Table 3 gives the sample-based 95/95 DNBR limit, to be compared with the licensed limits in Table 1. None of the correlations exhibits a systematic bias at the level of the whole database: the medians are 1.019, 1.024, and 0.985 for B&W-2, W-3, and WRB-1, all within 2.5% of unity. At this aggregate level, WRB-1, with the smallest σ_{ln} (0.157) and the lowest non-conservative fraction (44.4%), is the most favorable of the three for design use. W-3, in contrast, shows the largest σ_{ln} (0.196) with correspondingly heavier tails in Fig. 1, and this scatter places the sample-based 95/95 limits of W-3 and WRB-1 above their licensed values. Such an aggregate view, however, may conceal regional biases of opposite sign, and the heavy tails indicate that the prediction quality is not uniform over the parameter space.

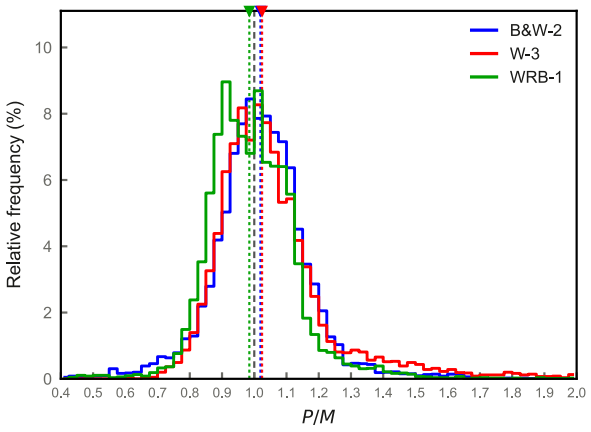


Fig. 1. *P/M* distributions of the three correlations on the common sample.

Table 3. Overall performance on the common sample.

Correlation	n	Median	σ_{ln}	NC (%)	95/95
B&W-2	8,525	1.019	0.165	56.1	1.26
W-3	8,525	1.024	0.196	56.3	1.53
WRB-1	8,525	0.985	0.157	44.4	1.24

4.2 Effect of the Axial Power Distribution

Table 4 examines the effect of the axial power distribution. Within each design region, uniform-heating cases were matched to peaked cases sharing the same test-section geometry and closely matched operating conditions (residual mismatches $|\Delta G| \leq 75$ kg/m²·s, $|\Delta P| \leq 0.05$ MPa, $|\Delta h_{sub}| \leq 86$ kJ/kg), and the median *P/M* shift from the uniform to the peaked distribution was evaluated; an asterisk marks shifts whose bootstrap 95% confidence interval excludes zero, i.e., shifts that are statistically significant. In the i-SMR region (uniform to bottom-peaked), the shift is at most +1.3% and statistically insignificant for all three correlations; in the PWR region (uniform to mid-peaked), the shifts lean toward the non-conservative side but are significant only for WRB-1 (+4.1%). The subsequent region comparison is therefore performed without a correction for the axial power distribution. The limited number of matched pairs sets the detection limit of this check at approximately 5%; an axial-peaking effect below this limit, even if present, is far smaller than the i-SMR-region bias and therefore cannot alter the region comparison.

Table 4. Median *P/M* shift (%) from uniform to peaked axial distributions.

Region	Contrast	n (Uni/Non)	B&W-2	W-3	WRB-1
i-SMR	uniform → bottom	15/8	+1.3	+0.6	−0.2
PWR	uniform → mid	6/13	+2.7	+4.3	+4.1*

4.3 Assessment in the Design Regions

Fig. 2 compares the *P/M* distributions in the i-SMR region (n = 877), in the full pressure-range sample (n = 4,839), and in the PWR region (n = 190), all on the HBM basis. The full-sample distributions retain the near-unity behavior of Fig. 1, and the PWR-region distributions remain centered close to unity. In the i-SMR region, in contrast, the distributions of all three correlations are shifted toward the non-conservative side as a whole (medians 1.094, 1.078, and 1.052 for B&W-2, W-3, and WRB-1).

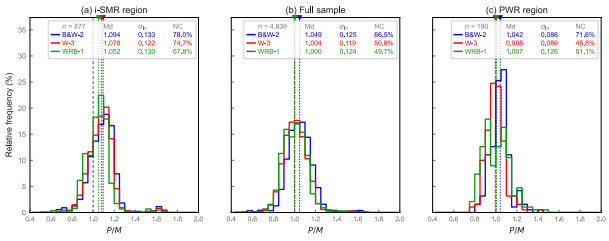


Fig. 2. *P/M* distributions in the i-SMR region, the full sample, and the PWR region.

Table 5 quantifies this shift; the in-range column denotes the fraction of the region cases that lie inside the applicability range of each correlation. In the i-SMR region, the non-conservative fractions reach 68–78%, i.e., approximately three quarters of the data points are overpredicted. WRB-1 is the closest to unity, but its 95/95 limit still exceeds the licensed value (1.23 vs 1.17). For W-3, only 45.7% of the region cases are in range, so that the assessment of this region is largely an extrapolation of the correlation. In the PWR region, the medians of W-3 and WRB-1 return to unity (0.995 and 1.007), which confirms that the i-SMR-region bias is a property of the region rather than of the database.

Table 5. Performance in the design regions.

Region	Corr.	In-range (%)	Median	σ_{ln}	NC (%)	95/95
i-SMR	B&W-2	72.6	1.094	0.133	78.0	1.26
(n = 877)	W-3	45.7	1.078	0.122	74.7	1.24
	WRB-1	96.7	1.052	0.130	67.8	1.23
All	B&W-2	69.0	1.049	0.125	66.5	1.24
(n = 4,839)	W-3	76.0	1.004	0.119	50.8	1.19
	WRB-1	93.3	1.000	0.124	49.7	1.20
PWR	B&W-2	84.7	1.042	0.086	71.6	1.26
(n = 190)	W-3	86.3	0.995	0.089	45.8	1.20
	WRB-1	99.5	1.007	0.126	51.1	1.31

Fig. 3 locates the weak region on the G–L plane. The cell boundaries are placed in the natural gaps of the test matrix, namely the nominal-mass-flux families and the untested heated-length bands, and the sample size is printed in each cell. The difficulty is shared by all three correlations: the non-conservative fraction is largest in the low-G column and peaks in the i-SMR cell ($G \leq$ 1,600 kg/m²·s, L = 2,134–2,438 mm) at 73–79%. Within this heated-length band, however, the fraction improves markedly as G increases — for WRB-1, the best-performing correlation, from 73% to 46% — although the heated length is unchanged. This behavior suggests that the weakness lies in the mass-flux dependence of the correlations, for which the i-SMR mass-flux range sits at the lower edge of every development database (Table 1), rather than in the heated length alone. Moreover, the mass flux appears explicitly in every published form of the three correlations, while the heated length appears in none of them. The refit was therefore performed on the mass-flux term, and the influence of the heated length was evaluated from the variation of the prediction performance with L after the refit.

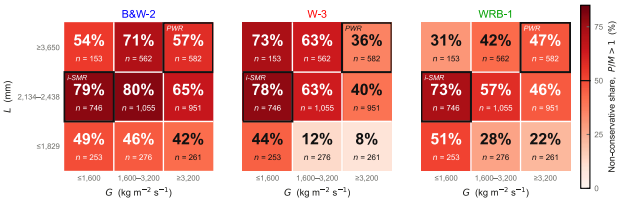


Fig. 3. Non-conservative fraction (P/M > 1) on the G–L plane.

4.4 Refit of the Mass-flux Term and Residual Structure

Table 6 and Fig. 4 present the refit result. The mass-flux term k_2 of W-3 (Eq. (6)) was refitted to the uniform-heating cases in the pressure range, for which the non-uniform correction reduces to a constant. Of these cases, 70% were used for fitting with region-balanced weighting and the remaining 30% for validation; the exponents p_1 and p_2 of B&W-2 (Eqs. (2) and (3)) were refitted in the same manner as a control. The refit changed k_2 as follows:

$$k_2 = \frac{(0.1484 - 1.596x + 0.1729x|x|)G}{10^6} + 1.037 \quad (11)$$

$$k_{2,new} = \frac{(0.2011 - 0.6248x + 0.7880x|x|)G}{10^6} + 0.8063 \quad (12)$$

Table 6. DSM P/M medians (σ_{ln}) on the validation set before and after the refit.

Correlation	Region	Original Md (σ_{ln})	Refit Md (σ_{ln})
W-3	i-SMR	1.185 (0.262)	1.073 (0.222)
	high-G	0.933 (0.215)	0.953 (0.196)
	All	1.021 (0.290)	0.982 (0.249)
B&W-2	i-SMR	1.278 (0.357)	1.256 (0.335)
	high-G	1.102 (0.215)	0.900 (0.218)
	All	1.175 (0.381)	1.024 (0.323)

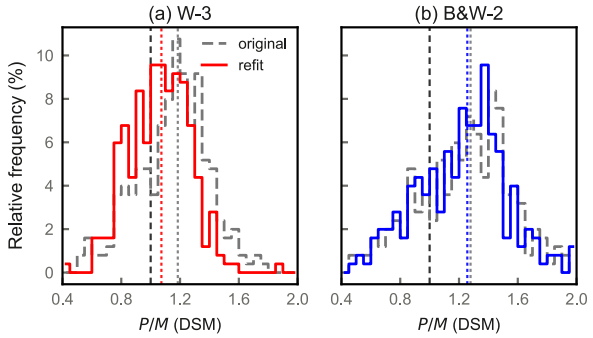


Fig. 4. DSM P/M distributions in the i-SMR region before and after the refit.

The change weakens the negative quality–mass-flux coupling and lowers the constant term, so that the predicted CHF decreases mainly at low mass flux. As a result, the i-SMR-region median improves from 1.185 to 1.073, while the high-G region and the overall scatter are preserved or improved (Table 6); the corresponding shift of the distribution toward unity is visible in Fig. 4(a). The same procedure leaves B&W-2 essentially unchanged in the i-SMR region and instead distorts the high-G region (Fig. 4(b)). The difference comes from the development databases: W-3, although it also lacks a heated-length term, was fitted over heated lengths of 254–3,658 mm, so the length effect could be partly absorbed into its other terms; B&W-2 was regressed at a single heated length (1,829 mm, Table 1), so the length effect could never enter the correlation, and refitting it with data of various lengths yields no visible improvement. The refit thus establishes that a database-coverage problem exists in the G-dependence of W-3 and that its correction removes a substantial part of the region bias.

Fig. 5 decomposes the refit sample by heated length within the i-SMR region; the medians are taken over all uniform-heating cases in the region, and the number of cases at each length is printed on the axis (only 17 cases at L = 2,438 mm). For W-3, the refit lowers the medians at all lengths together, while the spread between the lengths, approximately 0.35 in P/M, remains essentially unchanged; for B&W-2, the original and refitted lines nearly coincide. The residual rank correlations exhibit the same behavior: after the refit, the W-3 residual is nearly decorrelated from the mass flux (Spearman ρ = −0.26 → −0.07) and from the local quality (−0.41 → +0.05), whereas its correlation with the heated length strengthens (+0.25 → +0.54). The influence of the heated length is therefore evident, but the present functional form provides no means of reflecting it, because the heated length — or the grid geometry that accompanies it, which the present database cannot separate — is not a variable of the correlation. An improvement that incorporates the heated-length information is required for the i-SMR region.

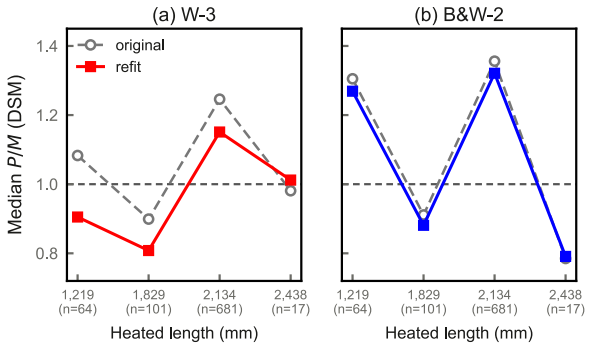


Fig. 5. Median DSM P/M by heated length in the i-SMR region before and after the refit.

5. Conclusion

The prediction performance of the B&W-2, W-3, and WRB-1 correlations was assessed against 8,525 rod-bundle CHF tests of the EPRI database, analyzed with the subchannel code MATRA, with attention to the i-SMR design region. Over the whole database the three correlations showed nearly unbiased medians, and WRB-1, with the smallest scatter, was confirmed to be the most favorable for design use. In the i-SMR design region, however, all three correlations were confirmed to be non-conservative: the medians reached 1.05–1.09, approximately three quarters of the data points were overpredicted, and the required 95/95 DNBR limit of WRB-1 exceeded its licensed value. This regional bias was shown not to originate from the mixture of axial power distributions, and its disappearance in the PWR region confirmed that it is tied to the i-SMR conditions themselves. On the G–L plane the non-conservative predictions concentrated at low mass flux, which lies at the lower edge of the development databases of all three correlations, and the non-conservative fraction improved markedly with increasing mass flux even at fixed heated length; the mass-flux dependence was thereby identified as the primary weakness. W-3, whose fully published and multiplicative form allows an individual term to be modified, was refitted in its mass-flux term: about 60% of the region bias was removed while the high-mass-flux region was preserved, which confirmed that this part of the bias is a database-coverage problem. Once the mass-flux influence was removed, the remaining bias followed the heated length distinctly — the residual correlation with L strengthened from +0.25 to +0.54 while the residual correlations with the mass flux and the quality vanished — and this is because none of the correlations contains the heated length as a variable; B&W-2, regressed at a single heated length, showed no improvement under the same refit. Therefore, for CHF prediction in the i-SMR design region, the mass-flux dependence can be corrected by refitting against data that cover the region, whereas the heated-length bias cannot be removed within the existing functional forms; an extension that incorporates the heated length is required, and its development is proposed as future work.

ACKNOWLEDGEMENT

This work was supported by the Innovative Small Modular Reactor Development Agency grant (No. RS-2023-00257680) and Nuclear Safety Research Program through the Korea Foundation of Nuclear Safety (KoFONS) and the Regulatory Research Management Agency for SMRs (RMAS) using the funding source granted by the Nuclear Safety and Security Commission (NSSC) of the Republic of Korea (Nos. RS-2026-25538149 and RS-2025-02309978).

REFERENCES

[1] L. S. Tong, "Boiling crisis and critical heat flux," USAEC Critical Review Series, Rep. TID-25887, U.S. Atomic Energy Commission, Oak Ridge, TN, USA, 1972.
[2] IAEA, Advanced Reactors Information System (ARIS), Design Status Report: i-SMR (iSMRDA/KHNP), Rep. DSR 109, Vienna, Austria, Oct. 2024.
[3] J. S. Gellerstedt, R. A. Lee, W. J. Oberjohn, R. H. Wilson, and L. J. Stanek, "Correlation of critical heat flux in a bundle cooled by pressurized water," in Two-Phase Flow and Heat Transfer in Rod Bundles (ASME Winter Annual Meeting, Los Angeles, CA, USA), V. E. Schrock, Ed. New York, NY, USA: ASME, Nov. 1969, pp. 63–71.
[4] F. E. Motley, K. W. Hill, F. F. Cadek, and J. Shefcheck, "New Westinghouse correlation WRB-1 for predicting critical heat flux in rod bundles with mixing vane grids," Westinghouse Electric Corp., Pittsburgh, PA, USA, Rep. WCAP-8762, Jul. 1976.
[5] C. F. Fighetti and D. G. Reddy, "Parametric study of CHF data, Vol. 3, Parts 1–2: Critical heat flux data," Electric Power Research Institute, Palo Alto, CA, USA, Rep. NP-2609, Sep. 1982.
[6] Y. J. Yoo, D. H. Hwang, and D. S. Sohn, "Development of a subchannel analysis code MATRA applicable to PWRs and ALWRs," J. Korean Nucl. Soc., vol. 31, no. 3, pp. 314–327, 1999.